Idris, N. A., Yoshizawa, K., Tomomatsu, Y., Sudo, M., Hajikano, T., Kubo, R., Zervas, G., & Tsuda, H. (2016). Full-mesh T- and O-band wavelength router based on arrayed waveguide gratings. *Optics Express*, *24*(1), 672-686. https://doi.org/10.1364/OE.24.000672

Full-mesh T- and O-band wavelength router based on arrayed waveguide gratings

Nazirul A. Idris,[1,*] Katsumi Yoshizawa,[2] Yasunori Tomomatsu,[3] Makoto Sudo,[4] Tadashi Hajikano,[4] Ryogo Kubo,[1] Georgios Zervas,[1,5] and Hiroyuki Tsuda[1]

[1]Gradute School of Science and Technology, Keio University,3-14-1 Hiyoshi, Kohoku-ku, Yokohama-shi, Kanagawa 223-8522, Japan
[2]Pioneer Micro Technology Corp., 465 Osato-cho, Kofu-shi, Yamanashi 400-0053, Japan
[3]Koshin Kogaku Co., Ltd., 69-3 Bodai, Hadano-shi, Kanagawa 259-1302, Japan
[4]Optoquest Co., Ltd.,1335 Haraichi, Ageo-shi, Saitama 362-0021, Japan
[5]HPN group University of Bristol,Bristol,BS8 1UB, UK
[*]nazafham273@tsud.elec.keio.ac.jp

Abstract: We propose an ultra-broadband full-mesh wavelength router supporting the T- and O-bands using 3 stages of cascaded arrayed waveguide gratings (AWGs). The router architecture is based on a combination of waveband and channel routing by coarse and fine AWGs, respectively. We fabricated several T-band-specific silica-based AWGs and quantum dot semiconductor optical ampliers as part of the router, and demonstrated 10 Gbps data transmission for several wavelengths throughout a range of 7.4 THz. The power penalties were below 1 dB. Wavelength routing was also demonstrated, where tuning time within a 9.4-nm-wide waveband was below 400 ms.

OCIS codes: (060.4265) Networks, wavelength routing; (200.4650) Optical interconnects; (080.1238) Array waveguide devices; (230.5590) Quantum-well, -wire and –dot devices; .

References and links

1. A. H. Gnauck, G. Charlet, P. Tran, P. Winzer, C. Doerr, J. Centanni, E. Burrows, T. Kawanishi, T. Sakamoto, and K. Higuma, "25.6-Tb/s WDM transmission of polarization-multiplexed RZ-DQPSK signals," J. Lightwave Technol. **26**(1), 79-84 (2008).
2. H. Liu, C.-F. Lam, and C. Johnson, "Scaling optical interconnects in datacenter networks - opportunities and challenges for WDM," in Proc. of 18th IEEE HOTI 2010, CA, USA, 113–116.
3. T. Pfeiffer, "New avenues of revenues: open access and infrastructure virtualization," in *National Fiber Optic Engineers Conference*, OSA Technical Digest (Optical Society of America, 2012), paper NTh4E.1.
4. N. Yamamoto and H. Sotobayashi, "All-band photonic transport system and its device technologies," in Proc. SPIE **7235**, 72350C (2009).
5. Y. Omigawa, N. Yamamoto, A. Kanno, T. Kawanishi, Y. Kurata, and H. Sotobayashi, "Polarization division multiplexed 4 × 10 Gbps simultaneous transmissions in 1.0-μm waveband and C-waveband over a 14.4.-km-long holey fiber using an ultra-broadband photonic transport system," Opt. Express **20**(14), 14864–14870 (2012).
6. N. Yamamoto, H. Sotobayashi, K. Akahane, and M. Tsuchiya, "Quantum-dot Fabry-Perot laser-diode with a 4-THz injection-seeding bandwidth for 1-μm optical-waveband WDM systems, " in Proc. of ISLC 2008, Sorrento, Italy, P20 (2008).
7. N. Yamamoto, K. Akahane, T. Kawanishi, R. Katouf, and H. Sotobayashi, "Quantum dot optical frequency comb laser with mode-selection technique for 1-μm waveband photonic transport system," Jpn. J. Appl. Phys. **49**, 04DG03 (2010).
8. N. Yamamoto, Y. Omigawa, Y. Kinoshita, A. Kanno, K. Akahane, T. Kawanishi, and H. Sotobayashi, "Development of broadband optical frequency resource over 8.4-THz in 1.0-μm waveband for photonic transport systems," Proc. SPIE **7958**, 79580F (2011).
9. H. Asakura and H. Tsuda, "Design and characterization of an arrayed-waveguide grating router with an interleave-chirped array," IEICE Electron. Express **12**(9), 1-6 (2015).
10. N. Yamamoto, K. Akahane, T. Kawanishi, Y. Omigawa, H. Sotobayashi, Y. Yoshioka, and H. Takai, "Narrow-line-width 1.31-μm wavelength tunable quantum dot laser using sandwiched sub-nano separator growth technique," Opt. Express **19**(26), B636-B644 (2011).

11. T. Akiyama, M. Ekawa, M. Sugawara, K. Kawaguchi, H. Sudo, A. Kuramata, H. Ebe, and Y. Arakawa, "An ultrawide-band semiconductor optical amplifier having an extremely high penalty-free output power of 23 dBm achieved with quantum dots," IEEE Photon. Technol. Lett. **17**(8), 1614-1616 (2005).
12. K. Kato, A. Okada, Y. Sakai, K. Noguchi, T. Sakamoto, S. Suzuki, A. Takahara, S. Kamei, A. Kaneko, and M. Matsuoka, "32 × 32 full-mesh (1024 path) wavelength-routing WDM network based on uniform-loss cyclic-frequency arrayed-waveguide grating," Electron. Lett. **36** (15), 1294-1296 (2000).
13. K. Noguchi, Y. Koike, H. Tanobe, K. Harada, and M. Matsuoka, "Field trial of full-mesh WDM network (AWG-STAR) in metropolitan/local area," J. Lightwave Technol. **22**(2), 329-336 (2004).
14. K. Noguchi, A. Okada, S. Kamei, S. Suzuki, and M. Matsuoka, "Temperature control-free full-mesh wavelength routing network (AWG-STAR) with CWDM AWG-router," J. Lightwave Technol. **23**(4), 1568-1575 (2005).
15. O. Moriwaki, K. Noguchi, T. Sakamoto, S. Kamei, and H. Takahashi, "Wavelength path reconfigurable AWG-STAR employing coprime-channel-cycle arrayed-waveguide gratings," IEEE Photon. Technol. Lett. **21**(14), 1005-1007 (2009).
16. Z. Xu, X. Cheng, Y.-K. Yeo, X. Shao, L. Zhou, and H. Zhang, "Large-scale WDM passive optical network based on cyclical AWG," Opt. Express **20**(13), 13939-13946 (2012).
17. F. Zhang, W.-D. Zhong, Z. Xu, T. H. Cheng, C. Michie, and I. Andonovic, "A broadcast/multicast-capable carrier-reuse WDM-PON," J. Lightwave Technol. **29**(15), 2276-2284 (2011).
18. K. Sato, H. Hasegawa, T. Niwa and T. Watanabe, "A large-scale wavelength routing optical switch for data center networks," IEEE Commun. Mag. **51**(9), 46-52 (2013).
19. K. Ueda, Y. Mori, H. Hasegawa, K. Sato, and T. Watanabe, "Large-scale optical-switch prototype compactly implemented with novel functional configuration," in *Optical Fiber Communication Conference*, OSA Technical Digest (online) (Optical Society of America, 2015), paper W3D.1.
20. Y.-K. Yeo, Z. Xu, D. Wang, J. Liu, Y. Wang, and T.-H. Cheng, "High-speed optical switch fabrics with large port count," Opt. Express **17**(13), 10990-10997 (2009).
21. K. Xi, Y.-H. Kao, and H. J. Chao, "A petabit bufferless optical switch for data center networks," in *Optical Interconnects for Future Data Center Networks*, C. Kachris, K. Bergman, and I. Tomkos, ed. (Springer, 2013).
22. X. Ye, Y. Yin, S. J. B. Yoo, P. Meija, R. Proietti, and V. Akella, "DOS – A scalable optical switch for datacenters," in Proc. of 6th ACM/IEEE ANCS 2010, CA, USA, paper 24.
23. R. Proietti, C. J. Nitta, Y. Yin, R. Yu, S. J. B. Yoo, and V. Akella, "Scalable and distributed contention resolution in AWGR-based data center switches using RSOA-based optical mutual exclusion," IEEE J. Select. Top. Quantum Electron. **19**(2), 3600111 (2013).
24. P. N. Ji, D. Qian, K. Kanonakis, C. Kachris, and I. Tomkos, "Design and evaluation of a flexible-bandwidth OFDM-based intra-data center interconnect," IEEE J. Select. Top. Quantum Electron. **19**(2), 3700310 (2013).
25. P. Bernasconi, C. Doerr, C. Dragone, M. Cappuzzo, E. Laskowski, and A. Paunescu, "Large $N \times N$ waveguide grating routers," J. Lightwave Technol. **18**(7), 985-991 (2000).
26. S. Kamei, M. Ishii, A. Kaneko, T. Shibata, and M. Itoh, "$N \times N$ cyclic-frequency router with improved performance based on arrayed-waveguide grating," J. Lightwave Technol. **27**(18), 4097-4104 (2009).
27. K. Takada, M. Abe, T. Shibata, and K. Okamoto, "A 25-GHz-spaced 1080-channel tandem multi/demultiplexer covering the *S*-, *C*-, and *L*-Bands using an arrayed-waveguide grating with gaussian passbands as a primary filter," IEEE Photon. Technol. Lett. **15**(5), 648-650 (2002).
28. K. Takada, M. Abe, T. Shibata, and K. Okamoto, "5 GHz-spaced 4200-channel two-stage tandem demultiplexer for ultra-multi-wavelength light source using supercontinuum generation," Electron. Lett. **38**(12), 572-573 (2002).
29. T. Kitoh, Y. Inoue, M. Itoh, M. Kotoku, and Y. Hibino, "Low chromatic-dispersion flat-top arrayed waveguide grating filter," Electron. Lett. **39** (15), 1116-1118 (2003).
30. H.-C. Lu and W.-S. Wang, "Cyclic arrayed waveguide grating devices with flat-top passband and uniform spectral response," IEEE Photon. Technol. Lett. **20**(1), 3-5 (2008).
31. K. Okamoto and H. Yamada, "Arrayed-waveguide grating multiplexer with flat spectral response," Opt. Lett. **20**(1), 43-45 (1995).
32. J.-J. He, "Phase-dithered waveguide grating with flat passband and sharp transitions," IEEE J. Select. Top. Quantum Electron. **8**(6), 1186-1193 (2002).
33. K. Maru, "Performance analysis of a synchronized-router-based flat-passband filter using multiple-input arrayed waveguide grating with phase errors," J. Lightwave Technol. **29**(13), 1965-1974 (2011).
34. C. R. Doerr, L. W. Stulz, and R. Pafchek, "Compact and low-loss integrated box-like passband multiplexer," IEEE Photon. Technol. Lett. **15**(7), 918-920 (2003).
35. C. R. Doerr, M. A. Cappuzzo, E. Y. Chen, A. Wong-Foy, L. T. Gomez, and L. L. Buhl, "Wideband arrayed waveguide grating with three low-loss maxima per passband," IEEE Photon. Technol. Lett. **18**(21), 2308-2310 (2006).
36. C. R. Doerr, M. Cappuzzo, L. Gomez, E. Chen, A. Wong-Foy, C. Ho, J. Lam, and K. McGreer, "Planar lightwave circuit eight-channel CWDM multiplexer with <3.9-dB insertion loss," J. Lightwave Technol. **23**(1), 62-65 (2005).
37. K. Jinguji and M. Oguma, "Optical half-band filters," J. Lightwave Technol. **18**(2), 252-259 (2000).

1. Introduction

Conventionally, development on optical communications have focused on the C- and L-bands due to the low optical power attenuation and the availability of high performance optical fiber amplifiers in these bands. The 11 THz of bandwidth of the C- and L-bands combined has been used extensively with the development of dense wavelength division multiplexing (DWDM), polarization multiplexing, and advanced modulation technologies [1]. However, a far wider bandwidth to the conventional bands would be a very promising solution. It could be utilized to implement scalable optical interconnects towards exascale datacenters [2] or a metro/access network system with various parallel services [3] using wavelength division multiplexing (WDM) technology. Recently, the T-band (Thousand-band:1.00–1.26 μm), which offers more than 60 THz worth of bandwidth, has been developed as a potential wavelength resource for an ultra-broadband short reach communications [4-9]. The relatively large optical power attenuation of optical fibers would constrain the reach of a system employed in this band, but the abundance of bandwidth would enable transmission capacity comparable to the conventional bands to be achieved with a more simpler configuration. Moreover, advances in quantum dot (QD)-based wavelength tunable lasers (WTLs) and semiconductor optical amplifiers (SOAs) with particularly wide gain bandwidth and flexibility in arranging the gain peak as desired further support the possibility of realizing ultra-broadband WDM systems operating in the T-band [10,11]. Recent reports regarding the T-band include a transmission line with a holey fiber structure being deployed for an all-band photonic transport system [5], various broadband laser sources based on QD structures [6-8], and arrayed waveguide grating (AWG)-based de/multiplexers [9].

Signal interconnection based on wavelength routing is the key for future high-capacity and low-latency WDM networks. In particular, a $N \times N$ passive wavelength router with full-mesh connection capability, usually in the form of an $N \times N$ cyclic AWG, is a very useful device that can be utilized in star-topology networks [12-15], large-scale and highly-functional WDM networks [16,17], optical interconnects in data center and high-performance computing [18-24], etc. However, the transmission properties of an AWG prevent it from being scaled up to a significant extent in terms of bandwidth for practical application in ultra-broadband WDM networks, mostly due to intrinsic passband peak deviation (PPD) from a uniformly spaced channel grid [25]. Various approaches on suppressing the PPD include a uniform-loss cyclic-frequency (ULCF) AWG configuration [12,26] and cascading multiple AWGs to form larger-scale full-mesh wavelength router [18,19,26].

In this paper, we propose a 3-stage AWG design to construct a highly scalable full-mesh wavelength router that completely encompasses the T- and O-bands, which has more than 79 THz of combined bandwidth. The wavelength router is based on a combination of waveband and channel routing using coarse (15.6 nm spacing) and (0.2 nm spacing) fine AWGs, respectively. Such routing configuration has previously been reported [27,28], where multiple fine AWGs are cascaded to a single coarse AWG to form a large-scale $1 \times N$ de/multiplexer. In our proposal of an $N \times N$ wavelength router, we use an array of fine AWGs sandwiched between an array of course AWGs on either side. This paper discusses in detail the router architecture, optical fiber configuration, and various considerations on designing the AWGs. We also demonstrate the feasibility of the 3-stage wavelength router by constructing parts of the router using T-band-specific AWGs and QD-based SOAs, as well as transmitting optical signals through the system. We measured bit error rate (BER) curves of the system and performed wavelength routing via wavelength tuning. The power penalties for several wavelengths throughout a range of 28 nm were around 0.5 dB to 1 dB and tuning time within a single 9.4-nm-wide waveband was below 400 ms.

2. 3-stage wavelength router configuration

Figure 1 shows a schematic diagram of an $N \times N$ non-blocking wavelength router. In this paper, we define an $N \times N$ wavelength router as a wavelength router with N input ports, N

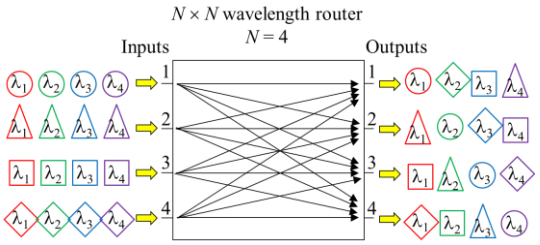

Fig. 1. Schematic diagram of an $N \times N$ non-blocking wavelength router.

output ports, and supports wavelength routing of N number of channels. In general, the fundamental requirements of this router can be described as follows:

- N number of wavelengths being input into each input port should be demultiplexed into N output ports.
- Each output port should multiplex N number of wavelengths, i.e. no identical wavelength should enter any single output port.

It is important to note that although the output wavelengths shown in Fig. 1 are arranged in a cyclical manner throughout all output ports, we do not consider the wavelength arrangement as a requirement for our wavelength router, i.e. it is acceptable for any wavelength from any input port to be output to any output port as long as both of the aforementioned conditions are satisfied. An $N \times N$ cyclic AWG is one of the most promising candidate for, and has widely been used as an $N \times N$ non-blocking wavelength router in various types of networks [12-24], as both of the aforementioned conditions can be innately satisfied by designing the free spectral range (FSR) to be N times the channel spacing, albeit having larger PPD from a uniformly spaced channel grid with larger channel count [25]. A non-uniform channel grid could mitigate the PPD, but fine wavelength tuning of laser sources to accommodate for the channel grid would be complicated. Furthermore, although cyclic AWGs with higher channel scalability have been proposed [12,26], chip size limitations would make fabrication of ultra-

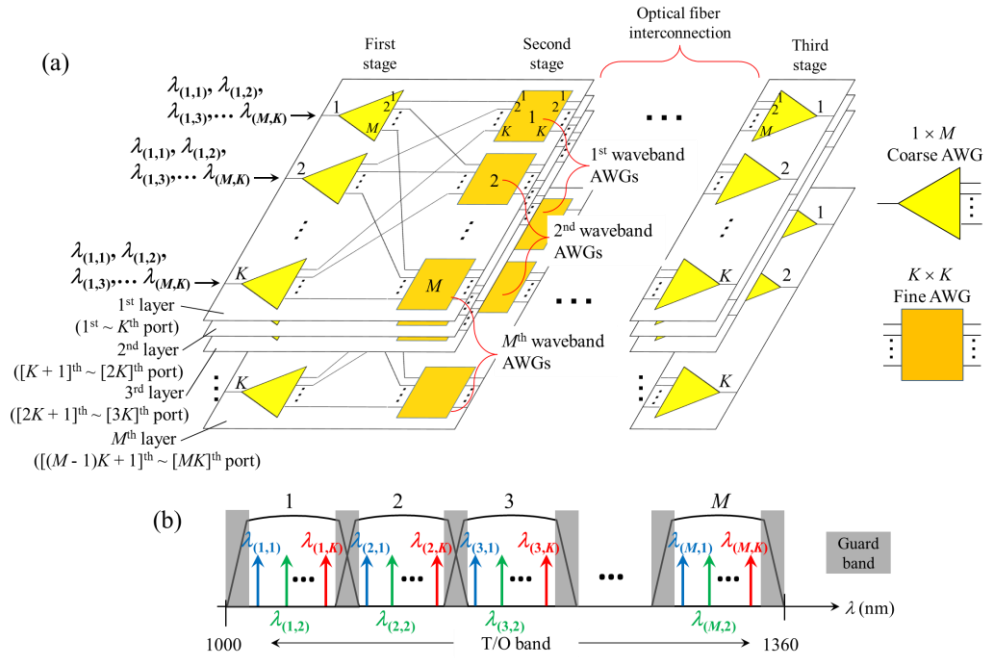

Fig. 2. (a) 3-stage $MK \times MK$ wavelength router architecture consisting of coarse and fine AWGs. (b) Allocation of M wavebands with K channels in each waveband. Here, $\lambda_{(m,k)}$ implies the k^{th} wavelength of the m^{th} waveband.

broadband cyclic AWGs suitable for T-band application practically impossible.

Therefore, we opted to cascade 3 stages of AWGs to form the desired wavelength router. The router architecture and channel allocation are depicted in Figs. 2(a) and 2(b), respectively. There are K channels in each of the M wavebands with a certain range of guard band between wavebands in which we will discuss the rationale later in subsection 3.2. This implies that the total number of supported channels for the wavelength router is $MK = N$. For viewing convenience, we illustrated the wavelength router architecture in the form of M number of layers. In each layer, there are K number of coarse AWGs for the first and third stages, and M number of fine AWGs for the second stage. The inputs of all the coarse AWGs in all of the layers represent different ports of the router, i.e. there is a total of MK number of ports. All of the coarse AWGs are identical, while the fine AWGs are waveband-specific, where in each layer there are M number of fine AWGs designed to support each of the M wavebands. If transmission signals are considered to travel from left to right, the first stage of coarse AWGs will separate MK number of channels into M wavebands and distribute each waveband to its corresponding fine AWG in the second stage. Each fine AWG will receive K channels of a single waveband from K number of different coarse AWGs and route all of the signals in a similar fashion to the $N \times N$ wavelength router shown in Fig. 1. The coarse AWGs on the third stage will then multiplex M wavebands, received from M number of fine AWGs of the second stage, onto a single output port, where there are K channels per waveband.

Optical fiber interconnections between the first and second stages of AWGs are done within each corresponding layer, i.e. no interconnection between different layers is required, and all layers have an identical layout. However, the interconnections between the second and the third stages of AWGs require inter-layer interconnections. Proper attention should be given in interconnecting the AWGs between the stages to ensure that a full-mesh wavelength router is achieved. In general, appropriate interconnections should satisfy the following conditions:

- Output ports of the m^{th} (m = 1, 2, 3,…M) fine AWG on the second stage should always be connected to the m^{th} input port of the coarse AWGs in the third stage.
- All MK number of output ports of all of the fine AWGs on the second stage of a particular layer should each be connected to MK number of different coarse AWGs on the third stage.

Figure 3 illustrates an example of appropriate interconnections for a 12 × 12 wavelength router, where K = 4 and M = 3. This way, the MK channels being input into each input port can be demultiplexed onto the MK output ports. The number of AWGs required for the first,

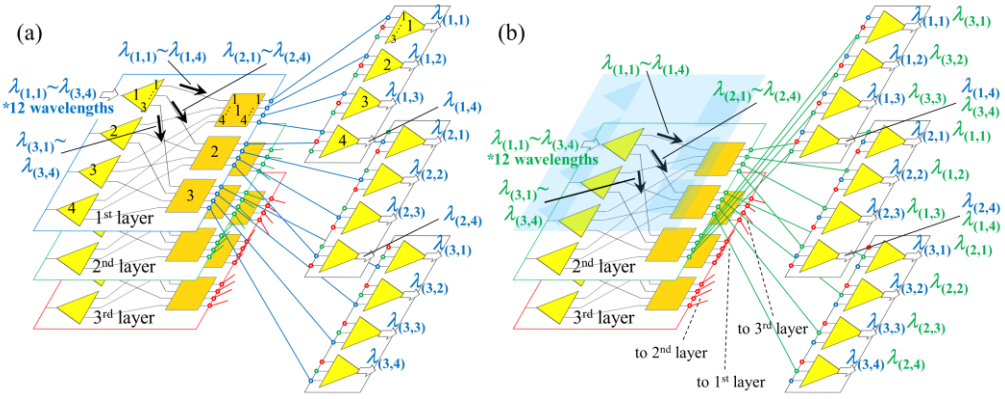

Fig. 3. Example of appropriate optical fiber interconnections between the fine AWGs on the second stage and the coarse AWGs on the third stage for a 12 × 12 wavelength router (M = 3, K = 4). (a) The output ports of the 1st, 2nd, and 3rd fine AWGs of the 1st layer are each connected to coarse AWGs on the 1st, 2nd, and 3rd layer, respectively. (b) The output ports of the 1st, 2nd, and 3rd fine AWGs of the 2nd layer are each connected to coarse AWGs on the 2nd, 3rd, and 1st layer, respectively. In a similar fashion, the output ports of the 1st, 2nd, and 3rd fine AWGs of the 3rd layer should be connected to coarse AWGs on the 3rd, 1st, and 2nd layer, respectively.

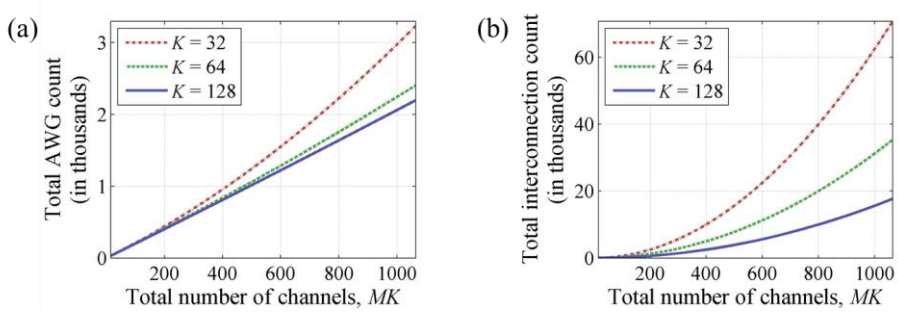

Fig. 4. Total number of (a) AWGs and (b) optical fiber interconnections required to construct an $MK \times MK$ wavelength router in the case of K = 32, 64, and 128.

second, and third stage to achieve full-mesh interconnection are MK, M^2, and MK, respectively, making a total of $2MK + M^2$ number of AWGs required for the wavelength router. On the other hand, the number of optical fiber interconnections required between any two stages, between 1st and 2nd or 2nd and 3rd, is M^2K, making the total number of interconnections $2M^2K$. Figures 4(a) and 4(b) show the total number of AWGs and optical fiber interconnections, respectively, required to construct a full-mesh wavelength router with MK number of channels using the proposed architecture. Note that it is critical that the number of channels of the fine AWGs, K, be as large as possible to reduce the total number of AWGs and interconnections required, and simplify the overall configuration. However, it is worth noting that increasing the channel count of an AWG generally causes the physical size to also increase, especially when supplementary components, such as the 2×1 couplers used in ULCF-AWG [12, 26], are needed for scaling up. There is also the possibility that multiple AWG chips could be integrated together to reduce the number of components, where the level of integration would generally depend on AWG size and layout. Therefore, these factors should also be considered when deciding M and K. Also, note that as the value of K approaches MK, the total number of AWGs will approach $2MK$, although obviously if a fine AWG with $K = MK$ number of channels could be realized, a full-mesh wavelength router could then be achieved using that single AWG.

3. Network specification considerations

3.1 Wavelength dependence properties of ultra-broad T- and O-bands

Designing an optical device able to operate in a combined broad bandwidth of T- and O-bands requires proper attention to the consequences of the very large wavelength dependent properties. Figures 5(a) and 5(b) show the calculated wavelength dependence of waveguide

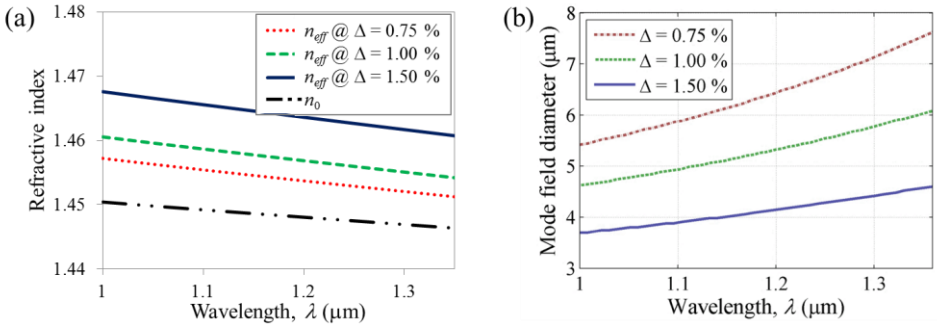

Fig. 5. (a) Waveguide core effective refractive index, n_{eff}, and (b) mode field diameter throughout T- and O-bands for Δ = 0.75%, 1.00%, and 1.50%. We assumed a square waveguide with a core width of 4.5 μm, 4 μm, and 3.2 μm for each Δ, respectively. Dash-dot-dot line in (a) show the cladding refractive index, n_0, which is assumed as pure silica, calculated using Sellmeier equation. All calculations with all Δ satisfying its corresponding value at λ = 1.0 μm.

core effective refractive index, n_{eff}, and mode field diameter (MFD) for 3 different refractive index differences, Δ = 0.75%, 1.00%, 1.50%, throughout T- and O-bands, where square waveguides with dimensions suitable to suppress multimode occurrence were assumed. The n_{eff} change from λ = 1.00 μm to λ = 1.36 μm was more than 0.006 for all Δ. The high wavelength dependence of n_{eff}, along with the value of wavelength itself, produces a wavelength-dependent propagation constant, which results in a highly-wavelength-dependent MFD. As shown in Fig. 5(b), the MFD expands around 1 μm, 1.3 μm, and 2.1 μm for Δ = 0.75%, 1.00%, and 1.50%, respectively, from λ = 1.00 μm to λ = 1.36 μm. This wavelength dependence of MFD is especially significant in that it restricts the usage of multimode-interference-based and directional-coupling-based waveguide structures, which is often used in adding certain functions or improving certain properties in a planar lightwave circuit (PLC), as both are very sensitive to the MFD of a propagating light.

3.2 Coarse AWG passband profile flattening for better spectral efficiency

When designing a system based on multiple channels within a waveband, a very crucial factor to consider is the achievable passband flatness of the coarse AWG. The less flat the passband is, i.e. the more it approaches the regular Gauss-like profile, the less uniform the insertion loss of the channels within that waveband will be. As such, channels at the edge of the band would suffer more losses and larger crosstalk than the central channels due to the curving nature of the passband. Therefore, we introduce a guard band region between neighbouring wavebands, as shown in Fig. 2(b). The guard band region represents a wavelength region where none of the wavelengths are used as a channel for the system, hence does not demand any level of transmission and crosstalk performance from the coarse AWG. The larger the 1-dB bandwidth to waveband spacing ratio for a coarse AWG could be achieved, the less guard band region is required, and the more spectral efficient the system will be.

Extensive studies have been done regarding AWG passband flattening that include using customized waveguide profiles at the slab boundary [29,30], non-uniform arrayed waveguides [31,32], multiple input waveguides connected to interferometers [33-35], and two interconnected AWGs with waveguide lenses [36]. Customizing waveguide profiles at the slab boundary requires the least physical space but the achievable flatness is quite limited [29,30]. It is also very sensitive to MFD as this technique generally involves multimode interference. A solution to the wavelength-dependent MFD is to employ customizations on the output waveguides (the waveguides where signals are separated into wavebands) instead of the input waveguide. This would allow each waveguide to be customized according to the average MFD of each waveband. On the other hand, using multiple input waveguide ports connected to interferometers offers better bandwidth but also suffers from MFD's wavelength dependency as it utilizes many directional couplers [33-35]. Interconnecting two AWGs with waveguide lenses is thought to be the most reliable when employed for an ultra-broad bandwidth as its mechanism does not involve any multimode interference and directional coupling [36]. It also allows very sharp passband transitions to be achieved, given that very large chip size is possible. Besides the aforementioned approaches, we could also consider employing a coarse AWG with very wide Gaussian passbands to enlarge the 1-dB bandwidth, and connect each of its output waveguides to waveband-specific bandpass filters, which can be constructed by cascaded mach-zehnder interferometers (MZI) [37], to reduce the crosstalk in neighbouring wavebands. The cascaded MZI also offers flat passbands with very sharp transitions given that very large number of MZI stages is allowed.

3.3 Suppressing PPD with appropriate channel spacing and channel count

Several other important considerations that should be determined in advance are whether to employ a channel grid equally spaced in wavelength or frequency, the channel spacing, Δf or $\Delta\lambda$, and the number of channels in each waveband, K, which are all correlated through their implication on the PPD of the AWGs. We calculated the maximum PPD, $\delta\lambda$ or δf, normalized to channel spacing, $\Delta\lambda$ or Δf, of AWGs with different parameters when used on cchannel grids

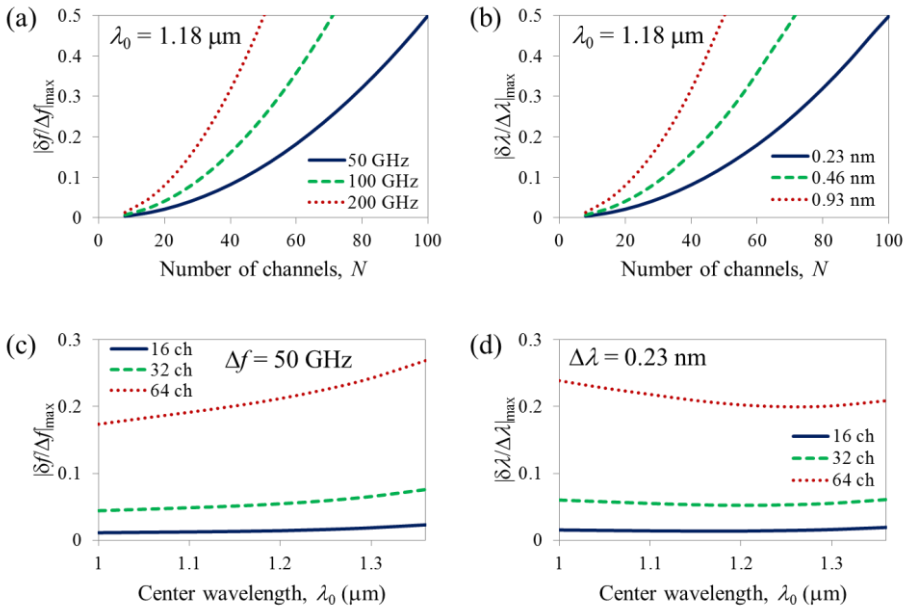

Fig. 6. Calculation results of maximum PPD, δf or $\delta\lambda$, normalized to channel spacing, Δf or $\Delta\lambda$. $|\delta f/\Delta f|_{max}$ = 1, and $|\delta\lambda/\Delta\lambda|_{max}$ = 1 correspond to a deviation that equals one channel spacing. Normalized deviation for grids equally spaced in (a) frequency and (b) wavelength when the center wavelength, λ_0 is fixed at 1.18 μm. Note that at λ_0 = 1.18 μm, wavelength spacing of 0.23 nm, 0.46 nm, and 0.93 nm approximately equal to 50 GHz, 100 GHz, and 200 GHz, respectively, in terms of frequency. Note also that we applied input and output waveguide shifts to all of the wavelength-based AWGs as suggested in [25] to reduce PPD. Normalized PPD for grids equally spaced in (c) frequency and (d) wavelength when the channel spacings, Δf and $\Delta\lambda$, are fixed at 50 GHz and 0.23 nm, respectively.

equally spaced in frequency and wavelength. Figure 6 shows the results, where normalized maximum PPD (PPD_{max}) is denoted as $|\delta f/\Delta f|_{max}$ or $|\delta\lambda/\Delta\lambda|_{max}$. In Figs. 6(a) and 6(b), it is apparent that the PPD_{max} rises with the number of channels and channel spacing, i.e. it rises with the amount of free spectral range (FSR) designed for the AWG. The number of channel, K, should then be as large as our system permits of the PPD_{max} to reduce the amount of AWG components required for the wavelength router, as discussed in section 2. Smaller channel spacing is preferable in reducing PPD, which is advantageous in terms of spectral efficiency. The limitation to channel spacing would then be crosstalk levels as in conventional AWG designing, where generally crosstalk level would be worse with smaller channel spacing.

The difference in using frequency- and wavelength-based channel grids are almost non-existent when the frequency and wavelength spacings are roughly equal to each other at center wavelength, λ_0. However, when the channel spacings are fixed, the PPD_{max} changes depending on the center wavelength of the AWG design, as shown in Figs. 6(c) and 6(d). In the T- and O-bands, for a grid equally spaced in frequency, larger wavelengths exhibit more PPD, while for a grid equally spaced in wavelength, the shortest wavelength exhibits the largest PPD. Decision on the number of channels and channel spacing should then be based on the wavelength with the most PPD. Based on these calculations, the PPD would not be an important factor on deciding whether to use a channel grid equally spaced in frequency or wavelength. However, as far as the network architecture proposed in this paper is concerned, the channel spacing of WTLs and the designing of coarse AWGs would be two important factors to consider. WTLs are usually spaced equally in frequency while AWG's diffractive characteristics naturally diffract equally spaced wavelength on roughly equal physical spacing. Therefore, channel grid equally spaced in frequency and wavelength are advantageous for easier design and fabrication of WTLs and coarse AWGs, respectively.

4. AWG fabrication and evaluation for T- and O-band wavelength router

Based on the considerations described in section 3, we propose a full-mesh T- and O-band wavelength router based on a channel grid equally spaced in wavelength. Table 1 shows the

Table 1. Design Parameters of the Coarse and Fine AWGs

Parameters	Coarse AWGs	Fine AWGs
Waveband number	-	1 ~ 23
Refractive index difference, Δ	≈ 1%	≈ 1%
Center wavelength, λ_0 (nm)	1179.4	1007.8 ~ 1351.0
Number of channels	M = 23	K = 47
Channel spacing, $\Delta\lambda$ (nm)	15.6	0.2
Diffraction order, m	2	106 ~ 141
Free spectral range (THz)	127.2	2.8 ~ 1.6 (≈ 9.4 nm)

design specifications of the coarse AWG and fine AWGs of all wavebands. The AWGs were based on silica waveguides with a Δ around 1.0%. All parameters are based on a spectral efficiency of 0.6 of the T- and O-bands, implying that 0.4 of the band will be assigned as guard bands. The value 0.6 was chosen based on previous reports of passband flattening, as described in subsection 3.2, and some calculations, in which it seemed reasonable when also taking account the AWG chip sizes and circuit layouts. The channel spacing of the grid is set to 0.2 nm. M and K are set to 23 and 47, respectively, making the wavelength router scalable up to 1081 channels with a total of 1,168,561 paths. Note that the channel spacing of the coarse AWG is 15.6 nm, while the FSR of the fine AWGs is only around 9.4 nm, which is approximately 0.6 of the coarse AWG channel spacing. Based on calculations, the normalized PPD_{max} of the fine AWGs for all wavebands ranges from 0.1 to 0.2.

We fabricated and evaluated several coarse and fine AWGs. The AWGs are silica waveguides deposited on a silicon substrate and were fabricated using standard photolithography techniques. We managed to laid out two coarse AWGs into a 3 cm squared chip. Two fine AWGs were also laid out into a 3 cm squared chip. The coarse AWGs were designed to have a very wide Gaussian passband with a 1-dB bandwidth that covers 0.6 of

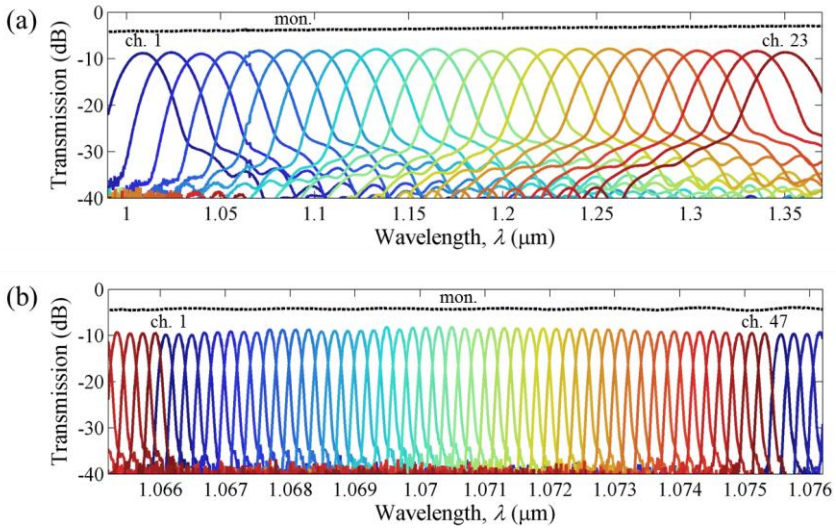

Fig. 7. Measured transmission spectra of the moduled (a) 1 × 23, 15.6-nm AWG and (b) 47 × 47, 0.2-nm AWG. mon. represents the transmission spectrum of monitor waveguides. The fine AWG shown in (b) is designed to operate at the 5th waveband.

every waveband, which is approximately 9.4 nm. This was achieved with a large tapered waveguide profile introduced at the input waveguide of the first slab. This design is with the assumption that waveband-specific bandpass filters based on cascaded MZI interferometers could be added to every output waveguide ports in the future for crosstalk suppression in neighbouring wavebands, as suggested in the previous section [37]. All AWGs were attached with optical fiber ribbon cables with a core diameter smaller than that of the C-band at the input and output ports. All of the fine AWGs are equipped with Peltier elements and thermistors to enable temperature tuning.

Figures 7(a) and 7(b) show a transmission spectra of each one of the moduled coarse and fine AWGs. For the coarse AWG, the fiber-to-chip coupling loss is aroung 4 dB to 5 dB, depending on the wavelength, and insertion loss ranges from 4.3 dB to 5.6 dB. 1-dB bandwidth ranges from 11.0 nm to 13.4 nm, which covers the 9.4 nm of operational bandwidth of each waveband. Figure 7(b) show the transmission spectra of a fine AWG designed for the 5th waveband. The center wavelength was designed to be at 1070.2 nm, but all of the passbands were shifted around +0.5 nm, mostly due to the mismatch between refractive indices used for calculation and the actual indices. Better accuracy is expected to be achieved in the future when feedbacks from current results are taken into account. The fiber-to-chip coupling loss is around 4 dB, and insertion loss ranges from 3.8 dB to 5.7 dB. Crosstalk at neighbouring channels was measured below -25 dB. We also measured the temperature dependence of the fine AWG, where the wavelength shifts were ±0.008 nm for every ±1 °C of temperature change. Another AWG module designed to operate in the 6th waveband also exhibits similar characteristics. Based on this measurement results, the total of the coupling loss and insertion loss of the entire 3-stage wavelength router could be approximated to range aournd 26 dB to 30 dB. Although we only fabricated fine AWG modules in only two wavebands, the silica-based PLC is a very mature and reliable technology where the AWG parameters could be controlled with relatively high precision, and therefore would allow the realization of fine AWGs in all of the wavebands. The relatively large fiber-to-chip coupling loss is thought to be due to imperfect alignment resulted from using a non-T-band-specific laser. Calculation results show that the theoretical coupling loss is below 1 dB for the combination of optical fiber diameter and waveguide width used in the fabricated AWGs, and thus indicates that the fiber-to-chip coupling loss of each AWG in every stages could possibly be reduced by around 3 dB with better alignment. The transmission loss of the AWG itself is also expected to be reduced by around 1 to 2 dB with better design, making the total possible loss reduction of the 3-stage wavelength router around 12 to 15 dB in future fabrication.

5. Experimental setup and system evaluation

5.1 Experimental setup

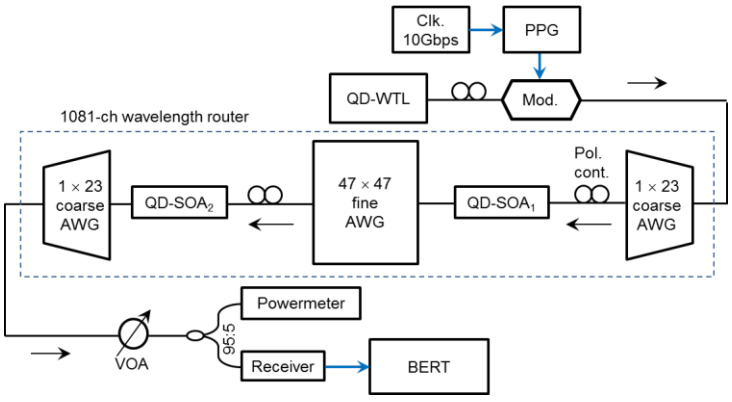

Fig. 8. Experimental setup for transmission demonstration of 1081-channel wavelength router.

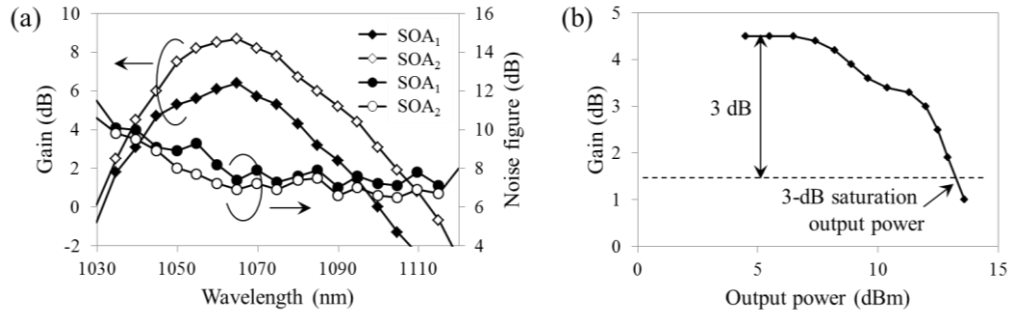

Fig. 9. (a) Gain and noise figure properties of the fabricated QD-SOAs when optical input power and injection current are -10 dB and 500 mA, respectively. (b) Gain-saturation characteristic and 3-dB gain saturation output power of QD-SOA_1 for λ = 1070.6 nm when injection current is 500 mA and optical input power is adjusted from 12.6 dBm to 0 dBm. On a side note, due to the insufficient optical power of our WTL, the gain-saturation characteristic of QD-SOA_1 was measured by firstly amplifying the optical power using QD-SOA_2. The lack of optical power also prevents us from measuring gain-saturation characteristics for other wavelengths.

To assess the feasibility of the proposed wavelength router, we set up the experimental testbed shown in Fig. 8. The transmitter consists of a QD-WTL, a T-band-specific modulator, and a pulse pattern generator (PPG). The part intended as the wavelength router consists of the fabricated coarse and fine AWGs, as well as two fabricated T-band-specific QD-SOAs for loss compensation. The gain chip of the QD-SOAs is composed of an InAs QD core layer sandwiched in between a p-AlGaAs and an n-AlGaAs layer on top and bottom of it, respectively, with the n-AlGaAs grown on an n-GaAs buffer layer and a GaAs substrate. The QD-SOAs that are constructed using these gain chips are based on a 2-lens system consisting of a fiber collimator and a focusing lens to realize a structure insensitive to optical axis deviation resulting from temperature changes. The influence of temperature changes was also reduced by placing the gain chip and the focusing lenses on the same heat sink. Figure 9(a) shows the gain and noise figure (NF) properties of those QD-SOAs measured when the input optical power and injection current were -10 dBm and 500 mA, respectively. The gain of QD-SOA_1 and QD-SOA_2 both peaks at around 1065 nm with a gain of 6.4 dB and 8.7 dB, respectively. The 3-dB gain bandwidth of SOA_1 and SOA_2 are approximately 44 nm and 40 nm, respectively. From shorter to longer wavelength, the NF of both SOAs varies from around 11 dB to 7 dB. To our knowledge, these are the first QD-SOAs fabricated to operate in this wavelength region. Figure 9(b) shows the gain-saturation characteristic of QD-SOA_1 for λ = 1070.6 nm. The 3-dB gain saturation output power was around 13 dBm. As shown in Fig. 8, QD-SOA_1 is placed between the first coarse AWG and the fine AWG, while QD-SOA_2 is placed between the fine AWG and the second coarse AWG.

The QD-WTL used as the optical source was also constructed using the same QD gain chip of the QD-SOAs. The QD-WTL is an external cavity laser consisting of the aforementioned QD gain chip, 3 pieces of band pass filters, and an etalon filter with 100-GHz of FSR, that realizes a 100-GHz spaced, single mode oscillation wavelength tuning ranging from 1030 nm to 1120 nm. The QD-WTL thus covers around 14 THz of the T-band, and covers from the 3rd to 7th wavebands of our proposed wavelength router. To our knowledge, it is also the first QD-WTL fabricated to operate in this wavelength region. Stabilization is performed by built-in isolator and temperature control mechanisms. The output power varies from 0 dBm to 8 dBm depending on the wavelength with the central region generally being higher. The typical laser linewidth (HWHM) is around 145 kHz. To manage optical polarization, polarization controllers were placed before the input of the modulator and both QD-SOAs. The QD-SOAs and QD-WTL are operated through a self-made application on a computer. All of the optical fibers used in this setup are single mode fibers with a core diameter of 5.8 μm, which is smaller than the conventional C-band single mode fibers, to prevent multimode occurrence for the shorter wavelength.

5.2 Transmission demonstration

We modulated the optical output of the QD-WTL with pseudo random binary sequence (PRBS) with a sequence length of 2^{15}-1 at 10 Gbps, injected the SOAs with 500 mA of current and measured bit error rate (BER) curves for various wavelength channels and routing paths. Figure 10 shows the measurement results. We achieved error free transmission for one wavelength in each of the 4th, 5th, and 6th wavebands, which are λ = 1054.8 nm, 1070.6 nm, and 1082.9 nm, respectively, as shown in Fig. 10(a). These wavelengths cover around 7.4 THz (≈ 28 nm) of the T-band. The wavelengths beyond this bandwidth lacked the optical transmittivity due to lower QD-WTL output power, lower QD-SOA gain, and higher AWG losses to enable error free transmission. We also achieved error free transmission for several wavelengths of the 5th waveband, as shown in Figs. 10(c) and 10(d), to confirm the feasibility of using all of the wavelength channels throughout the 9.4 nm of operational bandwidth in each waveband. On a side note, although the operational bandwidth of the 5th waveband is supposed to cover from 1066.0 nm to 1075.2 nm, we did not achieve error free transmission for wavelengths above 1073.6 nm due to the lack of optical transmittivity, i.e. losses of the coarse and fine AWGs are larger for the wavelengths at the edge of a waveband.

Furthermore, we also achieved error free transmission for several routing paths of λ = 1070.6 nm, as shown in Fig. 10(b), to confirm the feasibility of using various routing paths of the wavelength router. The power penalties for all of the wavelength channels that we

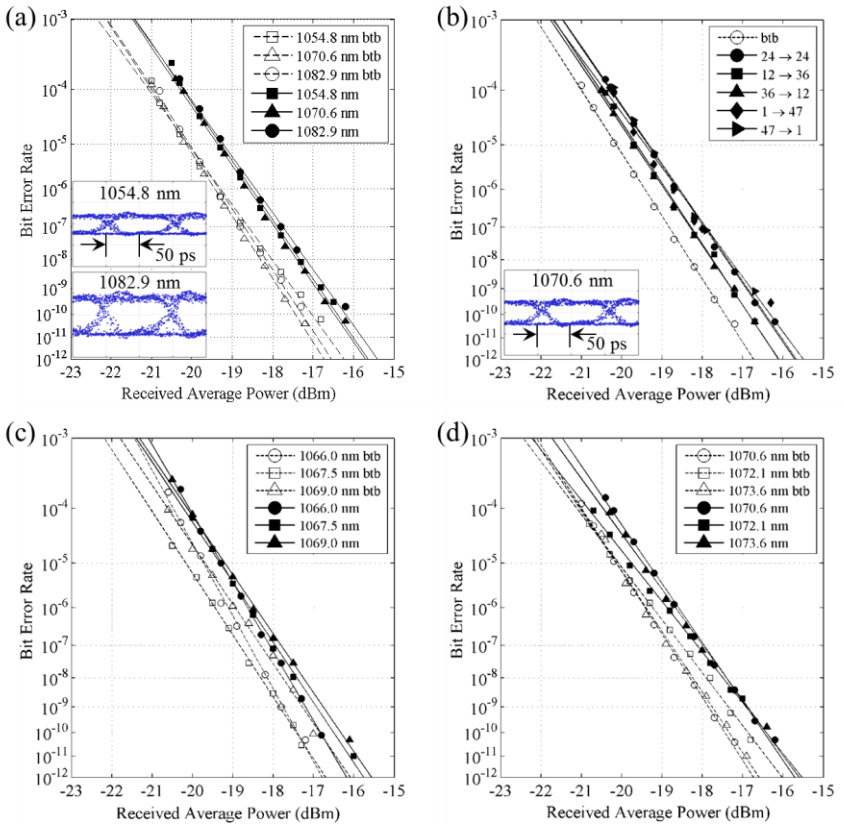

Fig. 10. Measured BER curves of several wavelength channels of the router and their back-to-back (btb) configuration. (a): One wavelength in each of the 4th, 5th, and 6th waveband. (b): λ = 1070.6 nm for 5 different routing paths (legend shows the input and output port numbers of the fine AWG). The inset in (a) and (b) show the eye patterns of the btb configuration for the three wavelengths shown in (a). On a side note, the O/E converter used for the eye pattern measurement was the conventional C-band-specific type. (c) and (d): Several wavelengths in the 5th waveband and their btb configuration when the input port of the fine AWG is fixed at the 24th.

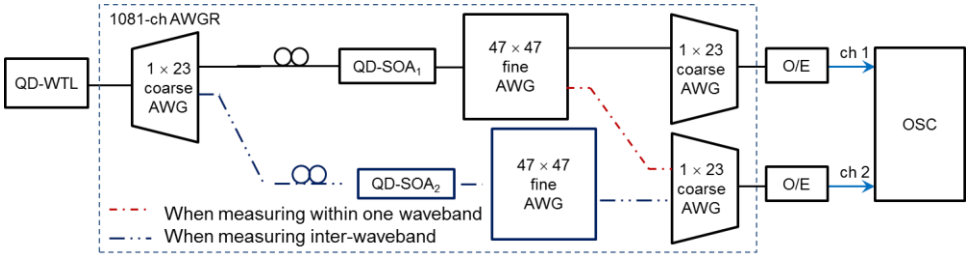

Fig. 11. Experimental setup for wavelength tuning measurement.

measured range from 0.5 dB to 1 dB. The relatively highly varied power penalties is thought to be mostly due to measurement inaccuracy caused by the instability of the QD-WTL optical output power and the modulator, which was not equipped with any temperature stabilization mechanism. Future fabrication of QD-WTLs, QD-SOAs, and AWGs with better optical power, gain, and transmittivity, and temperature-controlled modulators would provide better power margin and allow the range of error free transmission measurement to be much broader with better measurement accuracy. Ultimately, the expected transmission loss reduction of around 12 to 15 dB for the wavelength router in future fabrication, as stated in section 4, would render the SOAs entirely unnecessary for the wavelength router, which is how the device is intended to be, as managing the polarization of very large number of SOAs is impractical. Better optical output power of the QD-WTLs would then extend the reach of the network.

5.3 Wavelength routing demonstration

We set up the experimental testbed as shown in Fig. 11 to perform wavelength routing within a waveband and inter-wavebands. When measuring within a waveband, the output of the first coarse AWG is connected to a fine AWG, where two outputs of the fine AWGs are then connected to two different coarse AWGs. Both outputs from the coarse AWGs, which represent two users, are then each connected to an O/E converter and simultaneously monitored on an oscilloscope. When measuring inter-wavebands, two outputs of the first coarse AWG are connected to two different fine AWGs, where one output from each of the fine AWG is then connected to two different coarse AWGs. Outputs from the coarse AWGs are then connected to an oscilloscope. The port number of the first coarse AWG outputs and second coarse AWG input should be consistent to the waveband in measurement. Ideally, the fine AWGs should also be those that are designed specifically for each waveband in measurement. However, as we only fabricated fine AWGs designed for the 5th and 6th wavebands at the moment, we used those AWGs accordingly with the appropriate input and output ports that transmit the desired wavelengths. Temperature adjustments were also done accordingly to raise transmittivity to proper levels for the measurement. QD-SOA$_1$ and QD-SOA$_2$ are each placed before the two fine AWGs' input for loss compensation. Ideally, the outputs after the fine AWGs should also be incorporated with QD-SOAs to replicate the setup on Fig. 8, but we lacked the additional QD-SOAs, and our wavelength routing demonstration does not require modulated signal transmission and high optical power levels.

Figures 12(a) and 12(b) show examples of wavelength routing demonstration within a

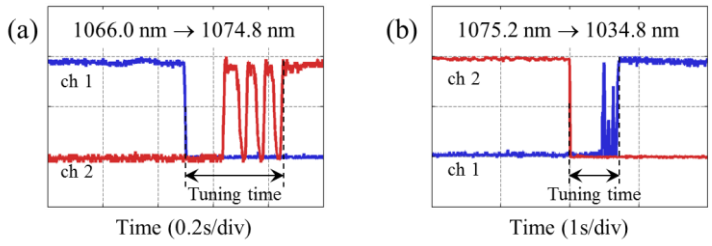

Fig. 12. Example of wavelength routing (a) within a waveband and (b) inter-wavebands.

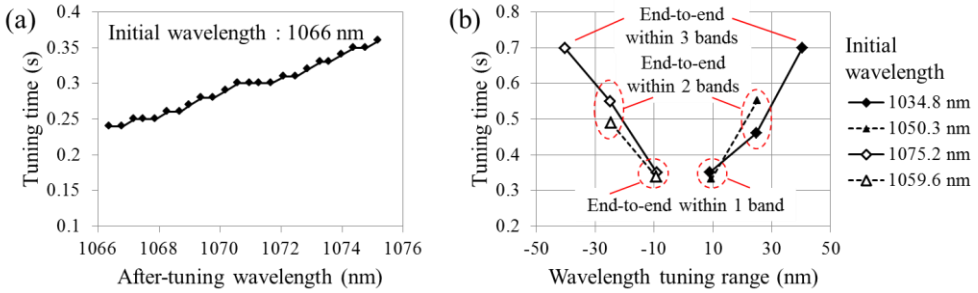

Fig. 13. Wavelength tuning time (a) within the 5th waveband when the initial wavelength is fixed at 1066 nm, and (b) inter-wavebands for various initial wavelengths. Below zero tuning range indicates wavelength tuning to wavelengths shorter than the initial wavelength.

waveband and inter-wavebands, respectively. The tuning time is measured from the point where the initial wavelength power falls to the point where the after-tuning wavelength power rises and maintains a stable state. The wavelength tuning time is mainly attributed to the QD-WTL having to adjust its bandpass filter angle, where larger wavelength tuning corresponds to larger angle adjustment, and a process of stabilizing the oscillation afterbandpass filter angle tuning, where a fixed amount of time is required everytime the wavelength is tuned. Figures 13(a) and 13(b) show wavelength tuning time within the 5th waveband and between three wavebands, respectively. The amount of time required to tune the wavelength from the shortest to longest wavelength within the 5th waveband was approximately 360 ms, with the tuning time increasing around 13.6 ms per 1 nm of wavelength shift. The end-to-end (shortest to longest or vice versa) wavelength tuning time within a single waveband, between 2 wavebands, and between 3 wavebands each averaged at approximately 350 ms, 500 ms, and 700 ms, respectively. Around 200 ms of each wavelength tuning time is attributed to the oscillation stabilization process, and is expected to be eliminated in future configuration. The time for bandpass filter angle adjustments is also expected to be cut in half, and thus shrinking the end-to-end wavelength tuning time within a single waveband, between 2 wavebands, and between 3 wavebands to approximately 75 ms, 150 ms, and 250 ms, respectively.

6. Conclusion

We proposed an ultra-broadband full-mesh non-blocking wavelength router scalable to encompass the entire 79 THz of bandwidth of the T- and O-bands combined. The wavelength router was implemented using 3 stages of cascaded coarse AWGs and fine AWGs and was based on a combination of waveband and channel routing. Based on various considerations, we designed the wavelength router to operate based on 23 wavebands and 47 channels within each waveband with a 0.2 nm channel spacing equally spaced in wavelength. The spectral efficiency of the proposed system was 0.6 as we introduced guard bands between the wavebands to relax the requirement of the coarse AWG passband flatness. The coarse AWG was designed to have a very wide 1-dB bandwidth. No AWG with particularly special modification were required to realize the proposed wavelength router.

We fabricated several silica-based coarse and fine AWGs with a Δ of around 1 % to evaluate the performance and demonstrate signal transmission through 3 stages of AWGs. The insertion loss of the coarse and fine AWGs were each around 4.3 dB to 5.6 dB and 3.8 dB to 5.7 dB, respectively. We also fabricated QD-based SOAs for loss compensation. The gain of QD-SOA1 and QD-SOA2 both peaks at around 1065 nm with a gain of 6.4 dB and 8.7 dB, respectively. The 3-dB gain bandwidth of QD-SOA_1 and QD-SOA_2 were approximately 44 nm and 40 nm, respectively. Furthermore, we fabricated a QD-WTL based on the same QD gain chip. The QD-WTL is 100-GHz-spaced tunable from 1030 nm to 1120 nm with an optical output power that varies between 0 dBm ~ 8 dBm. To demonstrate signal transmission, we setup a part of the wavelength router and modulated the optical signal with 10 Gbps of PRBS data. We achieved error free transmissions and measured the BER curves for most of

the wavelengths in the 5th waveband, and one wavelength each in the 4th and 6th wavebands. The power penalties for all those wavelength paths range around 0.5 dB to 1 dB. We also demonstrated wavelength routing and measured wavelength tuning time for cases of tuning within a single waveband and inter-wavebands. The end-to-end tuning time within a single waveband, between 2 wavebands, and between 3 wavebands each averaged at approximately 350 ms, 500 ms, and 700 ms, respectively.

Our measurements confirm the feasibility of using a 3-stage cascaded AWGs to realize a full-mesh wavelength router employed in the ultra-broad T- and O-bands using only conventional AWGs. Future works include improving QD-WTL optical power, QD-SOA gain, and AWG transmittivity to provide better power margin. Futhermore, considerations on utilizing AWGs with PPD suppressing structure should be made to reduce the number of AWG chips and interconnections. Further investigation on the best method of passband flattening suitable for this application should also be made to improve spectral efficiency. The number of wavebands and the number of channels in each waveband should then be optimized after considering the AWG layout, its chip size and level of integration, and AWG chip and interconnection count.

Acknowledgments

This work was funded by "Research and development on photonic networks using broad wavelength range of T-band and O-band," a commissioned research of the National Institute of Information and Communications Technology (NICT), Japan. The authors would like to extend their gratitude to Dr. Satoki Kawanishi of Photonic Crystal Laboratory, L.L.C. for his valuable suggestions and assistance in conducting the measurements described in this paper.